Generation of modal- and path-entangled photons using a domain-engineered integrated optical waveguide device

Jasleen Lugani,* Sankalpa Ghosh, and K. Thyagarajan
Department of Physics, Indian Institute of Technology Delhi, New Delhi 110 016, India
(Received 24 March 2011; published 24 June 2011)

Integrated optical devices are expected to play a promising role in the field of quantum information science and technology. In this paper we propose a scheme for the generation of nondegenerate, copolarized, modal, and path-entangled photons using a directional coupler and an asymmetric Y-coupler geometry in type-0 phase-matched domain-engineered lithium niobate (LN) waveguide. The nonlinearity in LN is tailored in such a way that quasi-phase-matching conditions for two different spontaneous parametric down-conversion processes are obeyed simultaneously, leading to a modal and path-entangled state at the output. Assuming typical values of various parameters, we show, through numerical simulations, that an almost maximally entangled state is achievable over a wide range of waveguide parameters. For the degenerate case, the proposed scheme gives a NOON state for $N = 2$. The generated entangled photon pairs should have potential applications in quantum information schemes and also in quantum metrology. By appropriate domain engineering and component designing, the idea can be further extended to generate hyperentangled and two-photon multipath-entangled states, which may have further applications in quantum computation protocols.

DOI: 10.1103/PhysRevA.83.062333 PACS number(s): 03.67.Bg, 42.65.Wi

I. INTRODUCTION

Quantum entangled photons, owing to their unique properties, play a crucial role in the implementation of quantum information protocols, quantum teleportation [1–3], and quantum computing [4,5]. The entanglement of photons can be exhibited in terms of their polarization, which is intrinsically binary, or spatial and spectral degrees of freedom, which are continuous variables. An important class of entangled photon states is NOON states or path-entangled states, defined as $|\mathcal{N}\rangle = \frac{1}{\sqrt{2}}(|N,0\rangle_{a,b} + |0,N\rangle_{a,b})$, which is the coherent superposition of N photons in two different spatial modes a and b. Nowadays, such NOON states are being exploited to beat the classical Rayleigh diffraction limit and thus to find potential applications in quantum metrology, imaging, and lithographic techniques [6–8].

The process of spontaneous parametric down-conversion (SPDC) in second-order ($\chi^{(2)}$) nonlinear bulk crystals and waveguides is a well-established method for the generation of polarization-entangled [9–12] and time-bin entangled photons pairs [13,14]. The use of waveguide structures leads to enhanced nonlinear efficiencies due to tight confinement of the interacting waves and provides a means to control the spatial characteristics of the down-converted photons by confining them to well-defined discrete transverse spatial modes [15,16]. This is in contrast to the continuous spatial distribution governed by momentum conservation in bulk crystals. By restricting the modes of the waveguide structure to the two lowest-order modes, the mode number can serve as a modal qubit [17], which can be used as an alternative to a polarization qubit. The guided-wave down-converted photon pairs can thus be emitted in the two allowed modes leading to modal entanglement. Such waveguide structures are also compatible with integrated optics technology and form basic components in photonic circuit designs, which are expected to play an important role in quantum information technology, owing to the compactness of the device and low loss. The generation, separation, and processing of entangled photons can be carried out on a single chip and hence the entangled photon state is less susceptible to decoherence. The photonic circuits based on titanium-indiffused channel lithium niobate (LN) waveguides have also been investigated recently for different combinations of modal, spectral, and polarization-entangled photon pairs [18,19].

In this paper we address the issue of generation of a modal and path-entangled state using SPDC in a domain-engineered integrated optical waveguide device. Several schemes have been proposed over the years to generate two-photon and multiphoton path entanglement using the SPDC process with the use of interferometric setups consisting of polarization beam splitters or Mach-Zehnder interferometers [20–22] and cavity QED [23]. We propose a scheme for the generation of a nondegenerate, copolarized modal-entangled state using a directional coupler in a type-0 phase-matched doubly periodically polarized LN waveguide. The nonlinearity in LN is tailored in such a way that quasi-phase-matching (QPM) conditions for two different SPDC processes are obeyed simultaneously [24]. These two SPDC processes, when enabled together, lead to a mode-entangled output state. We have shown through quantum-mechanical analysis and numerical simulations that for our choice of waveguide geometry and modes, maximally mode-entangled photon pairs can be achieved for a wide range of input parameters of the waveguide. Using an asymmetric Y coupler at the output, it is then possible to convert the mode-entangled state to a path-entangled state. The use of the directional coupler in our scheme facilitates the choice of the modes required, which leads to an appreciable overlap of the fields at the pump, signal, and idler wavelengths. The overlap integrals, which primarily determine the down-conversion efficiency, are quite high in comparison to a two-mode waveguide, giving rise to a high

*jaslphy@gmail.com

photon pair generation rate. Also, due to the design of the structure, we show that an efficient generation of photon pairs is possible using the fundamental spatial mode of the pump as compared to earlier work in which the first excited spatial mode had to be chosen in order to achieve good efficiencies [17]. The proposed device is flexible and the waveguide parameters can be modified to generate a hyperentangled state or a multipath-entangled state.

The organization of the paper is as follows. In Sec. II we describe the theory and the design of the integrated optical waveguide geometry considered for the generation of the mode-entangled state and the conversion of it to a path-entangled state. In Sec. III we give a brief account of the basic quantum-mechanical analysis for the two coupled SPDC processes involved in the generation of the desired mode-entangled state. In Sec. IV we present the results of numerical simulations and quantify entanglement by calculating the von Neumann entropy of the output state and show that a maximally entangled state is achievable using the proposed device. We also investigate the emission bandwidths of the two corresponding SPDC processes. We conclude with a brief summary in Sec. V.

II. WAVEGUIDE GEOMETRY

We seek to generate a mode-entangled state using spontaneous parametric down-conversion process in which the signal and idler photons are generated in an entangled pair of modes. Once generated, such a mode-entangled state can be converted to a path-entangled state such that if one of the down-converted photons comes out of one of the two (or more) available paths the other photon (generated with the first photon) would also come out of the same path and similarly for the other path(s). In order to achieve this we consider a waveguide geometry as shown in Fig. 1. Region I is a single-mode waveguide at the pump wavelength, followed by region II consisting of a symmetric Y splitter. Region III is a directional coupler supporting the fundamental (symmetric) normal mode and the first excited (antisymmetric) normal mode at signal and idler wavelengths. Using an appropriate phase matching in the directional coupler region, it is possible to generate down-converted photons that are entangled in mode number.

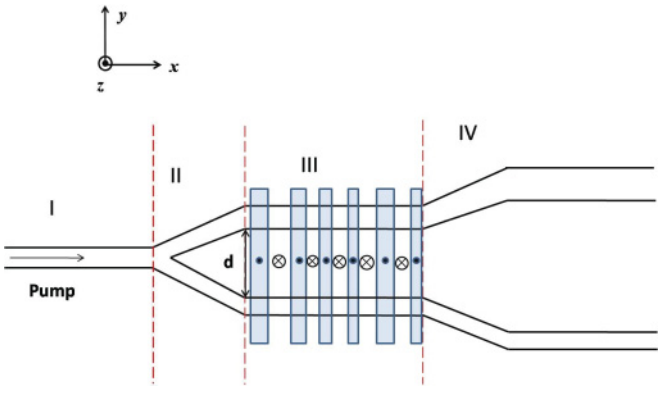

FIG. 1. (Color online) Waveguide design for generating modal and path-entangled photons. Region I is a single-mode waveguide at the pump wavelength, region II is a symmetric Y splitter, region III is a directional coupler consisting of a doubly periodic grating in the LN substrate (dots and crosses represent the polarizing directions in the grating), and region IV is an asymmetric Y coupler. The pump, signal, and idler are all z polarized, with the z axis being the optic axis for the LN substrate.

The proposed device works as follows. When the fundamental mode at the pump enters the input waveguide, it passes through the symmetric Y splitter and excites the fundamental symmetric normal mode at the pump wavelength in the directional coupler (region III). The directional coupler region is assumed to have a doubly periodic domain-reversal grating that simultaneously satisfies the QPM conditions [24] for two different SPDC processes: down-conversion of the pump photon in the fundamental normal spatial mode into signal and idler photons either (i) both in the fundamental normal spatial mode or (ii) both in the first excited normal spatial mode. The substrate used in this region is assumed to be a domain-engineered LN substrate that results in type-0 phase-matched down-conversion.

We show in Sec. III that satisfying the QPM conditions for both SPDC processes simultaneously will lead to the generation of a mode-entangled signal-idler photon pair in the doubly reversed region. Thus, in contrast to the standard phase matching based on a single process in either the bulk or the waveguide configuration, domain engineering can lead to the direct production of a copolarized mode-entangled state without the need for an interferometric setup or a 50:50 beam splitter.

To convert the mode-entangled state to a path-entangled state, at the output of the domain-reversed region, we have assumed an asymmetric Y coupler in region IV with both of the output waveguides being single mode and the propagation constant of the upper waveguide being higher than the lower waveguide for the signal and idler frequencies. Thus the fundamental normal modes of the signal and idler exit the upper waveguide while the first excited normal modes exit the lower waveguide leading to a path-entangled state. We show through numerical simulations that with an appropriate choice of parameters of the coupler it is possible to optimize the generation of the entangled state. In Sec. III we present a brief account of the quantum-mechanical analysis leading to the generation of a two-photon two-mode-entangled state in directional coupler region (region III of Fig. 1).

III. QUANTUM-MECHANICAL ANALYSIS

We consider the process of parametric down-conversion in a z-cut, x-propagating, domain-engineered lithium niobate waveguide. We assume the pump, signal, and idler wavelengths to all have extraordinary polarization to make use of the largest nonlinear coefficient d_{33} of lithium niobate. For the pump powers considered, the pump field is assumed to be a classical field and the signal and idler fields are represented by quantum-mechanical operators. The electric-field distributions for the pump [fundamental normal mode (0)], signal [fundamental (0) and first excited (1) normal modes], and idler [fundamental (0)

and first excited (1) normal modes] are given by the following:
Pump(0):

$$\vec{E}_{p0} = \tfrac{1}{2} e_{p0}(\vec{r})\, E_{p0}(e^{i(\beta_{p0}x-\omega_p t)} + e^{-i(\beta_{p0}x-\omega_p t)})\hat{z}, \quad (1)$$

Signal(0):

$$\hat{E}_{s0} = i\int d\omega_s e_{s0}(\vec{r})\sqrt{\frac{\hbar\omega_s}{2\epsilon_{s0}L}}(\hat{a}_{s0}e^{i\beta_{s0}x} - \hat{a}^{\dagger}_{s0}e^{-i\beta_{s0}x})\hat{z}, \quad (2)$$

Signal(1):

$$\hat{E}_{s1} = i\int d\omega_s e_{s1}(\vec{r})\sqrt{\frac{\hbar\omega_s}{2\epsilon_{s1}L}}(\hat{a}_{s1}e^{i\beta_{s1}x} - \hat{a}^{\dagger}_{s1}e^{-i\beta_{s1}x})\hat{z}, \quad (3)$$

Idler(0):

$$\hat{E}_{i0} = i\int d\omega_i e_{i0}(\vec{r})\sqrt{\frac{\hbar\omega_i}{2\epsilon_{i0}L}}(\hat{a}_{i0}e^{i\beta_{i0}x} - \hat{a}^{\dagger}_{i0}e^{-i\beta_{i0}x})\hat{z}, \quad (4)$$

Idler(1):

$$\hat{E}_{i1} = i\int d\omega_i e_{i1}(\vec{r})\sqrt{\frac{\hbar\omega_i}{2\epsilon_{i1}L}}(\hat{a}_{i1}e^{i\beta_{i1}x} - \hat{a}^{\dagger}_{i1}e^{-i\beta_{i1}x})\hat{z}, \quad (5)$$

where the subscripts 0 and 1 refer to the fundamental and first excited modes, respectively; $e_{p0}(\vec{r})$, $e_{s0}(\vec{r})$, and $e_{i0}(\vec{r})$ represent the transverse dependence of the fundamental modal fields of the pump (p), signal (s) and idler (i), respectively; $e_{s1}(\vec{r})$ and $e_{i1}(\vec{r})$ represent the transverse dependence of the first excited modal fields for the signal (s) and idler (i) wavelengths, respectively; L represents the interaction length; $\epsilon_{s0(1)}$ and $\epsilon_{i0(1)}$ correspond to optical dielectric permittivity of LN at signal and idler wavelengths for the fundamental and first excited mode; $\hat{a}_{s0}$ ($\hat{a}_{s1}$) and $\hat{a}_{i0}$ ($\hat{a}_{i1}$) represent the quantum-mechanical annihilation operators corresponding to the fundamental mode (first excited mode) of the signal and idler, respectively; β_{q0} ($q = p,s,i$) corresponds to the propagation constant for the fundamental mode; and β_{r1} ($r = s,i$) corresponds to the propagation constant for the first excited mode at the respective wavelengths. Energy is conserved for both processes such that $\omega_p = \omega_s + \omega_i$ with ω_p, ω_s, and ω_i being the pump, signal, and idler frequencies, respectively.

In order that the output state is entangled, the nonlinearity of the LN substrate in the directional coupler region is engineered to satisfy the following two QPM conditions simultaneously:

$$K_1 = \frac{2\pi}{\Lambda_1} = \beta_{p0} - \beta_{s0} - \beta_{i0}, \quad (6)$$

$$K_2 = \frac{2\pi}{\Lambda_2} = \beta_{p0} - \beta_{s1} - \beta_{i1}, \quad (7)$$

where Λ_1 and Λ_2 are the QPM grating periods for the individual SPDC processes. The second-order nonlinear polarization generated in the medium is given by

$$P_i^{\mathrm{NL}} = 2\epsilon_0 \sum_{j,k} d_{ijk} E_j E_k, \quad (8)$$

where the indices i,j,k (1,2,3) correspond to the components x,y,z of the coordinate system. Thus E_j represents the jth component of the total electric field within the medium and d_{ijk} is the corresponding nonlinear coefficient. For the case under consideration, the components of the total electric field are

$$\begin{aligned} E_1 &= 0, \\ E_2 &= 0, \\ E_3 &= \hat{E}_{p0} + \hat{E}_{s0} + \hat{E}_{s1} + \hat{E}_{i0} + \hat{E}_{i1}. \end{aligned} \quad (9)$$

The interaction Hamiltonian is derived as [24]

$$\hat{H}_{\mathrm{int}} = -4\epsilon_0 \int\int\int d_{33}(\hat{E}_{p0}\hat{E}_{s0}\hat{E}_{i0} + \hat{E}_{p0}\hat{E}_{s1}\hat{E}_{i1})dx\,dy\,dz. \quad (10)$$

Using the expressions for the electric fields defined in Eqs. (1)–(5), in the rotating-wave approximation and for energy conservation, we obtain the following expression for the interaction Hamiltonian:

$$\begin{aligned} \hat{H}_{\mathrm{int}} = \int d\omega_s \left(\frac{E_{p0}\hbar\sqrt{\omega_s\omega_i}}{L}\right)\int_0^L d_{33}\Bigg[\left(\frac{I_0}{n_{s0}n_{i0}}\right) \\ \times (\hat{a}^{\dagger}_{s0}\hat{a}^{\dagger}_{i0}e^{i[(\beta_{p0}-\beta_{s0}-\beta_{i0})x-\omega_p t]} \\ + \hat{a}_{s0}\hat{a}_{i0}e^{-i[(\beta_{p0}-\beta_{s0}-\beta_{i0})x-\omega_p t]}) \\ + \left(\frac{I_1}{n_{s1}n_{i1}}\right)(\hat{a}^{\dagger}_{s1}\hat{a}^{\dagger}_{i1}e^{i[(\beta_{p0}-\beta_{s1}-\beta_{i1})x-\omega_p t]} \\ + \hat{a}_{s1}\hat{a}_{i1}e^{-i[(\beta_{p0}-\beta_{s1}-\beta_{i1})x-\omega_p t]})\Bigg]dx, \end{aligned} \quad (11)$$

where I_0 and I_1 denote the overlap integrals of the electric-field profiles of the pump, signal, and idler modes involved in the two SPDC processes and are given as

$$I_0 = \int\int e_{p0}(\vec{r})\, e_{s0}(\vec{r})\, e_{i0}(\vec{r})\, dy\, dz, \quad (12)$$

$$I_1 = \int\int e_{p0}(\vec{r})\, e_{s1}(\vec{r})\, e_{i1}(\vec{r})\, dy\, dz. \quad (13)$$

The domain engineering in the LN substrate results in two independent spatial frequency components in the nonlinear coefficient variation, along the propagation direction [24]. Thus the effective nonlinear coefficient d including the effect of periodic domain reversal is given as

$$\bar{d}_{33} = -\frac{4d_{33}}{\pi^2}(e^{iK_1x} + e^{-iK_1x} - e^{iK_2x} - e^{-iK_2x}) + \mathcal{T}, \quad (14)$$

where $\mathcal{T}$ denotes terms at other spatial frequencies. By replacing d_{33} with $\bar{d}_{33}$ in Eq. (11) and simplifying, the interaction Hamiltonian in the interaction picture is obtained as

$$\hat{H}_{\mathrm{int}} = \int d\omega_s [C_0'(\hat{a}^{\dagger}_{s0}\hat{a}^{\dagger}_{i0} + \hat{a}_{s0}\hat{a}_{i0}) + C_1'(\hat{a}^{\dagger}_{s1}\hat{a}^{\dagger}_{i1} + \hat{a}_{s1}\hat{a}_{i1})], \quad (15)$$

where

$$C_0' = -\left(\frac{4d_{33}\hbar\sqrt{\omega_s\omega_i}\, I_0 E_{p0}}{\pi^2 n_{s0}n_{i0}}\right)e^{-i\Delta k_0 L/2}\mathrm{sinc}\left(\frac{\Delta k_0 L}{2}\right), \quad (16)$$

$$C_1' = -\left(\frac{4d_{33}\hbar\sqrt{\omega_s\omega_i}\, I_1 E_{p0}}{\pi^2 n_{s1}n_{i1}}\right)e^{-i\Delta k_1 L/2}\mathrm{sinc}\left(\frac{\Delta k_1 L}{2}\right), \quad (17)$$

and Δk_0 and Δk_1 are phase mismatch for the two processes given by

$$\Delta k_0 = K_1 - \beta_{p0} + \beta_{s0} + \beta_{i0}, \quad (18)$$

$$\Delta k_1 = K_2 - \beta_{p0} + \beta_{s1} + \beta_{i1}. \quad (19)$$

The output two-photon state is found to be

$$|\psi\rangle = \int d\omega_s i(C_0\,|s_0,i_0\rangle + C_1\,|s_1,i_1\rangle), \tag{20}$$

which is entangled; $C_0 = -(t/h)C_0'$ and $C_1 = -(t/h)C_1'$. The relative magnitudes of C_0 and C_1 coefficients will determine if the state is maximally entangled. These in turn depend upon the overlap integrals and the effective indices of the interacting modes at the pump, signal, and idler wavelengths. In Sec. IV we carry out simulations for a planar waveguide and using practical values of waveguide parameters we investigate various aspects of the output entangled state.

IV. NUMERICAL SIMULATIONS

In this section we report the results of simulations of the entangled states generated in the directional coupler region using a titanium-indiffused domain-engineered planar lithium niobate waveguide. We model region III as shown in Fig. 2. In order to demonstrate the generation of the entangled state in this region, we assume the planar waveguide to have step refractive index profiles. Since actual devices will use channel waveguides, our analysis can be used by first representing the channel waveguides by equivalent planar waveguides using the standard effective index method [25]. The analysis presented can be easily extended to waveguide geometries with graded refractive index profiles; however the general conclusions of our analysis would still be valid. As shown in Fig. 2, the guiding regions ($d/2 < |y| < a$) are assumed to have refractive index n_1 and the surrounding medium to have a refractive index n_2 ($<n_1$). Thus the geometry acts like a directional coupler with the cores of the individual waveguides separated by distance d. The individual core widths are $a - d/2 = r$. Modal analysis for the coupler region was carried out [26] and the eigenvalue equations for the symmetric and antisymmetric modes were obtained. The solution of these eigenvalue equations gives the propagation constants of all the modes at all the wavelengths. For the numerical simulations, the refractive indices of the substrate at the corresponding wavelengths have been calculated using temperature-dependent Sellmeier equation for LN [27]. The pump, signal, and idler wavelengths are chosen to be 750, 1452, and 1550 nm, respectively, and the corresponding refractive index differences $n_1 - n_2$ are assumed to be 0.0033, 0.0026, and 0.0025, respectively [24,28].

The propagation constants evaluated for the symmetric and antisymmetric modes at the signal and idler wavelengths vary with the core separation d as shown in Fig. 3. We can see from Fig. 3 that, as expected, beyond a certain core separation in the coupler region, the symmetric and antisymmetric modes have almost the same propagation constants for both the signal and idler wavelengths.

The transverse electric-field distributions of the interacting modes at the pump, signal, and idler are shown in Fig. 4 for a core separation of 6 μm. Figure 4(a) shows the electric-field distributions corresponding to the fundamental symmetric modes in the directional coupler region at the pump (solid line), signal (dashed line), and idler (dotted line) wavelengths and Fig. 4(b) shows the field distributions corresponding to the fundamental symmetric mode of the pump (solid line) and the first excited antisymmetric modes at the signal (dashed line) and idler (dotted line) wavelengths. The pump field is more tightly confined than the signal and idler wavelengths due to its shorter wavelength. Due to the choice of the waveguide geometry and wavelengths, it can be seen from the figure that there is a significant overlap between the fields of the interacting modes at the respective wavelengths, resulting in high down-conversion efficiencies for both of the SPDC processes.

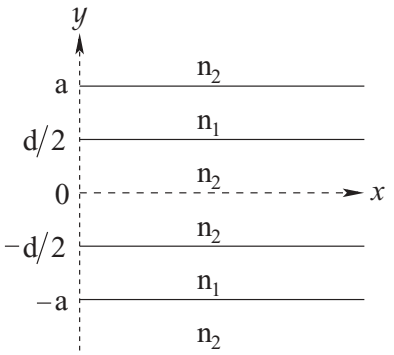

FIG. 2. Waveguide directional coupler geometry corresponding to region III of Fig. 1.

From the field expressions for the spatial modes at the pump, signal, and idler, we have evaluated analytical expressions for the overlap integrals I_0 and I_1 [defined by Eqs. (12) and (13)], which are plotted with respect to the core separation in Fig. 5. The figure shows that with an appropriate choice of waveguide separation, it is possible to obtain the desired ratios of the overlap integrals that lead to a high degree of entanglement between the down-converted photons.

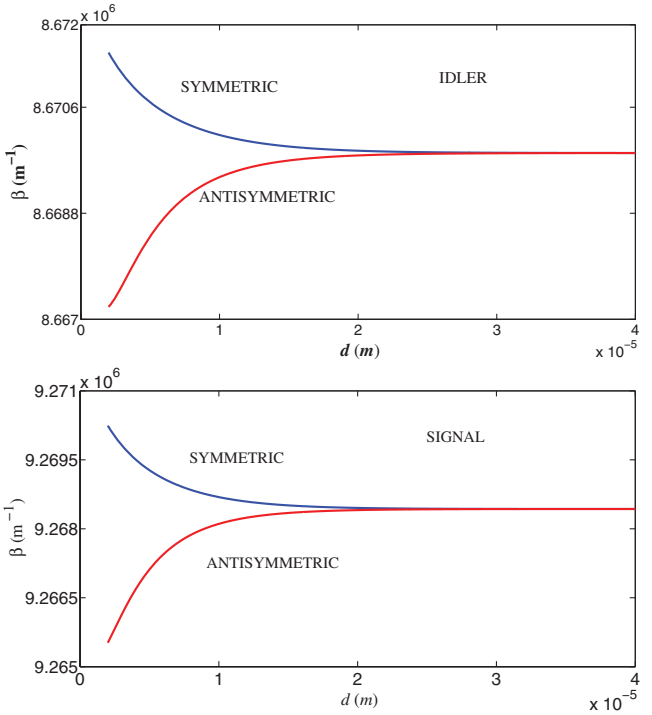

FIG. 3. (Color online) Variation of propagation constant with the core separation d corresponding to the (a) signal and (b) idler.

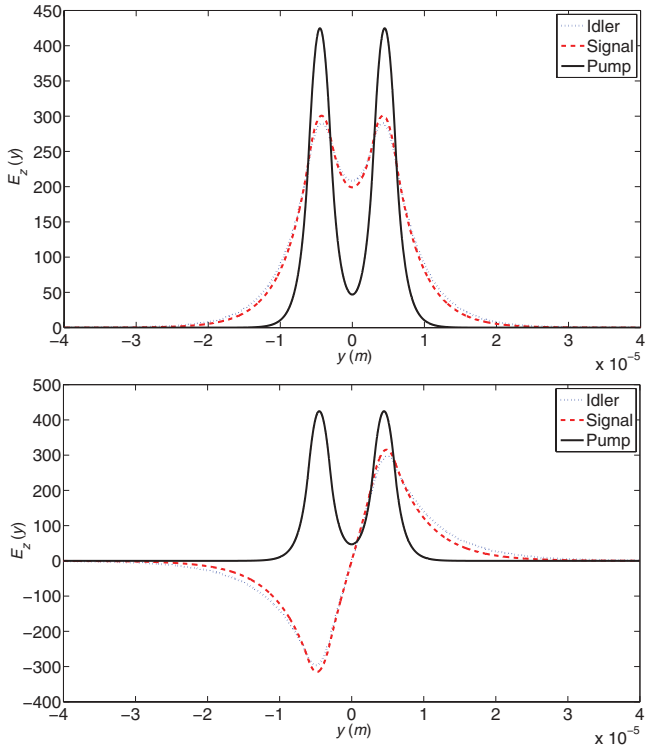

FIG. 4. (Color online) Normalized transverse electric-field distributions in the direction coupler region corresponding to (a) fundamental symmetric normal modes at the pump, signal, and idler wavelengths and (b) fundamental symmetric normal mode at the pump and first excited antisymmetric normal mode at the signal and idler wavelengths.

In order to quantify the entanglement, we calculate the von Neumann entropy [29] for the case of a perfectly phase-matched output entangled state of Eq. (20) (after normalization) as $S = -\mathrm{tr}(\rho^s \log_2 \rho^s)$ (with tr denoting the trace and ρ^s the reduced density matrix of the signal s photon), which is derived as

$$S = -\frac{I_0^2}{I_0^2 + I_1^2} \log_2 \frac{I_0^2}{I_0^2 + I_1^2} - \frac{I_1^2}{I_0^2 + I_1^2} \log_2 \frac{I_1^2}{I_0^2 + I_1^2}. \quad (21)$$

The variation of S with the waveguide separation is plotted in Fig. 6. The von Neumann entropy S for a maximally

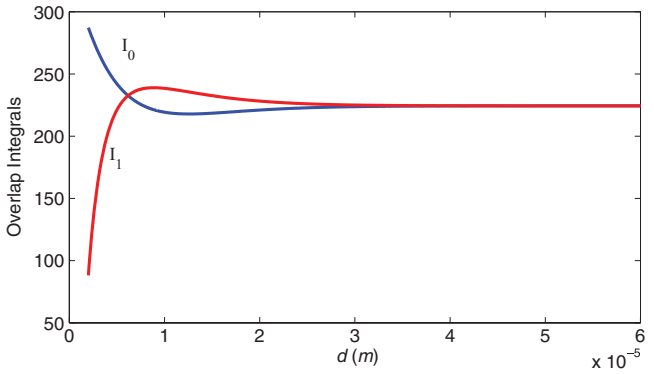

FIG. 5. (Color online) Variation of the overlap integrals with the core separation d.

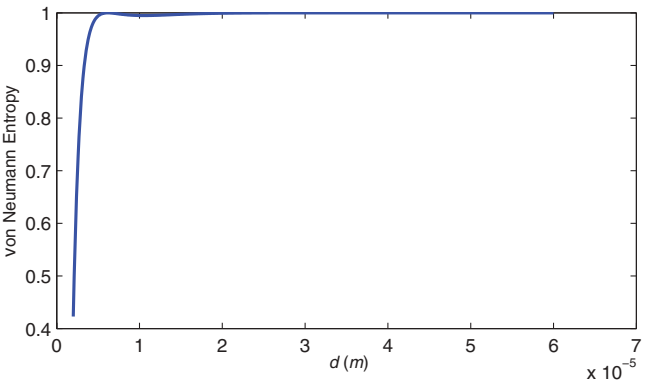

FIG. 6. (Color online) Variation of the von Neumann entropy with the core separation d.

entangled state is 1 and for a product state it is 0. We can see from Fig. 6 that for the entangled state generated using the proposed waveguide device, S becomes almost unity beyond a waveguide separation of about 6 μm, thus the device is capable of producing a maximally entangled state over a wide range of waveguide separation. The corresponding grating periods required for the two SPDC processes at this core separation are 17.521 and 17.358 μm, respectively, as calculated from Eqs. (6) and (7). Another condition for obtaining a maximally entangled state with high efficiency requires identical bandwidths for the two enabled SPDC processes [24]. Figure 7 shows the output spectra at signal wavelength corresponding to both of the SPDC processes. It can be seen from the figure that the two processes have almost identical bandwidths (16 nm), thus ensuring a maximally entangled state over the region of overlap [17].

We mention here that the above simulations have been carried out using a titanium-indiffused waveguide; simulations can also be performed for proton exchange LN waveguides, which may further increase the efficiencies due to tighter confinement of the modes. Thus, in region III we achieve two-photon modal entanglement. In the proposed device, this mode-entangled state is converted further to a path-entangled state when the photons reach region IV, which consists of an asymmetric Y coupler where, owing to the difference in the propagation constants of the upper and lower waveguides, the fundamental modes of the signal and idler would exit from

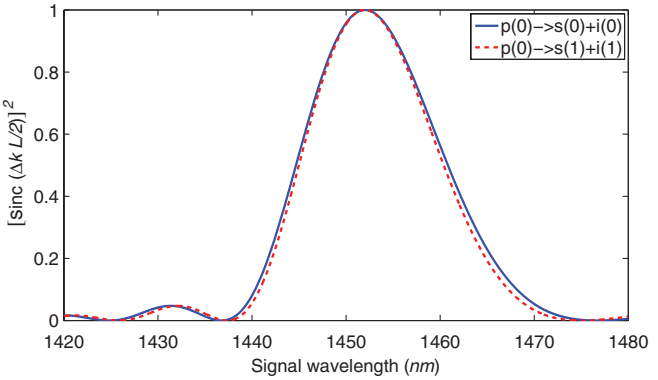

FIG. 7. (Color online) Normalized output signal spectra corresponding to the two SPDC processes considered.

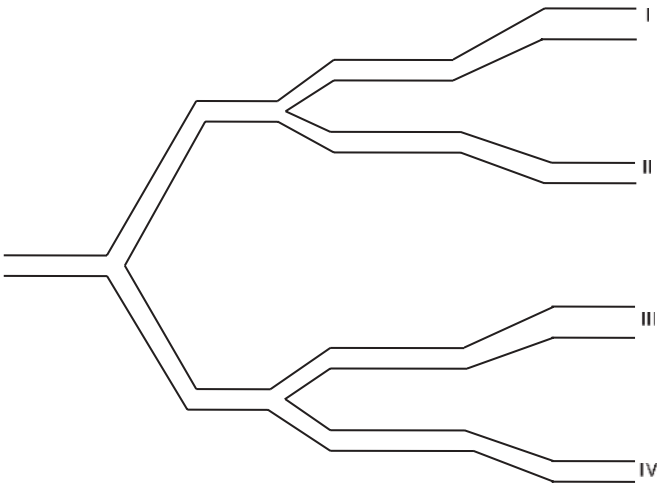

FIG. 8. Waveguide geometry for generating a four-path-entangled state.

the upper waveguide while the first excited modes would exit from the lower waveguide. This leads to a path-entangled state of the form

$$|\psi\rangle = \int d\omega_s i(C_0\,|s_u,i_u\rangle + C_1\,|s_l,i_l\rangle\,, \tag{22}$$

where the subscripts u and l correspond to the upper and lower waveguides, respectively. Thus both the signal and idler photons would exit from either the upper waveguide (fundamental mode) or the lower waveguide (first excited mode), thus resulting in path entanglement. If the SPDC process is chosen to lead to a degenerate pair of photons, then the output from the device would be a NOON state with $N = 2$. By modifying the waveguide parameters, the above scheme can be extended to generate different combinations of modal, polarization-, and path-entangled states giving rise to a hyperentangled state. Also, it can be used to generate a multipath-entangled state by appropriately engineering the phase-matching grating in the coupler region and enabling multiple SPDC processes simultaneously. This would lead to the generation of higher-order modes giving rise to a multimode, two-photon entangled state. The output Y coupler can then be fabricated with more than two output ports, correspondingly giving rise to a multipath, two-photon entangled state.

The multipath-entangled state can also be achieved by combining more of these above geometries and designing the structure appropriately. As an example, a four-path two-photon entangled state can be generated by designing the structure as shown in Fig. 8. Two of the waveguides of Fig. 1 are combined using a symmetric Y-coupler at the input and the signal-idler photon pair can exit from any of the four available paths with equal probability, giving rise to a maximally multi(four, in this case)-path entangled state. The potential applications for such multipath-entangled states have already been discussed in Ref. [30].

V. CONCLUSION

In this paper we have addressed the issue of generation of mode-entangled photon pairs using optical waveguide geometry, which has the inherent advantage of being compact (making the photons less susceptible to decoherence) and having enhanced optical nonlinearities in comparison to bulk crystal or optical fibers. The proposed scheme is very efficient as the pump, signal and idler are all taken to be extraordinarily polarized thus making use of the highest non linear coefficient d_{33} of lithium niobate; furthermore, due to our choice of geometry and the modes, the overlap integrals determining the efficiency of the two processes are also significant. We have shown that a maximally entangled state is achievable for a wide range of core separation of the coupler, with the additional advantage that one of the entangled photons is emitted at a typical wavelength of 1550 nm and can be used as a flying qubit. This mode-entangled state can be converted further to a path-entangled state, which should have varied applications in quantum lithography and quantum information processing. When the proposal is extended to degenerate SPDC processes it would lead to the production of a NOON state with $N = 2$ photons. By appropriately choosing the waveguide parameters and also designing the integrated structure, the idea is applicable to the production of a hyperentangled state and a multipath two-photon entangled state, which may have applications in quantum computation protocols.

ACKNOWLEDGEMENT

The work of J.L. was supported by University Grants Commission, New Delhi, India.

[1] D. Bouwmeester, J. Pan, K. Mattle, M. Eibl, H. Weinfurter, and A. Zeilinger, Nature (London) **390**, 575 (1997).
[2] S. L. Braunstein and H. J. Kimble, Phys. Rev. Lett. **80**, 869 (1998).
[3] A. Furusawa, J. Sorensen, S. Bruanstein, C. Fuchs, H. Kimble, and E. S. Polzik, Science **282**, 706 (1998).
[4] E. Knill, R. Laflamme, and G. J. Milburn, Nature (London) **409**, 46 (2001).
[5] P. Walther, K. J. Resch, T. Rudolph, E. Schenck, H. Weinfurter, V. Vedral, and M. Aspelmeyer, and A. Zeilinger, Nature (London) **434**, 169 (2005).
[6] A. N. Boto, P. Kok, D. S. Abrams, S. L. Braunstein, C. P. Williams, and J. P. Dowling, Phys. Rev. Lett. **85**, 2733 (2000).
[7] P. Kok, A. N. Boto, D. S. Abrams, C. P. Williams, S. L. Braunstein, and J. P. Dowling, Phys. Rev. A **63**, 063407 (2001).

[8] M. D'Angelo, M. V. Chekhova, and Y. Shih, Phys. Rev. Lett. **87**, 013602 (2001).
[9] P. G. Kwiat, K. Mattle, H. Weinfurter, A. Zeilinger, A. V. Sergienko, and Y. Shih, Phys. Rev. Lett. **75**, 4337 (1995).
[10] M. Fiorentino, G. Messin, C. E. Kuklewicz, F. N. C. Wong, and J. H. Shapiro, Phys. Rev. A **69**, 041801(R) (2004).
[11] A. Fedrizzi, T. Herbst, A. Poppe, T. Jennewein, and A. Zeilinger, Opt. Express **15**, 15377 (2007).
[12] A. Martin, V. Cristofori, P. Aboussouam, H. Hermann, W. Sohler, D. B. Ostrowsky, O. Alibart, and S. Tanzilli, Opt. Express **17**, 1033 (2009).
[13] R. T. Thew, S. Tanzilli, W. Tittel, H. Zbinden, and N. Gisin, Phys. Rev. A **66**, 062304 (2002).
[14] T. Honjo, H. Takesue, and K. Inoue, Opt. Express **15**, 1679 (2007).
[15] K. Banaszek, A. B. U'Ren, and I. A. Walmsley, Opt. Lett. **26**, 1367 (2001).
[16] A. Eckstein and C. Silberhorn, Opt. Lett. **33**, 1825 (2008).
[17] M. F. Saleh, B. E. A. Saleh, and M. C. Teich, Phys. Rev. A **79**, 053842 (2009).
[18] M. F. Saleh, G. Di Giuseppe, B. E. A. Saleh, and M. C. Teich, IEEE Photon. J. **2**, 736 (2010).
[19] M. F. Saleh, G. Di Giuseppe, B. E. A. Saleh, and M. C. Teich, Opt. Express **18**, 20475 (2010).
[20] C. C. Gerry and R. A. Campos, Phys. Rev. A **64**, 063814 (2001).
[21] P. Walther, J. W. Pan, M. Aspelmeyer, R. Ursin, S. Gasparoni, and A. Zeilinger, Nature (London) **429**, 158 (2004).
[22] S. Sauge, M. Swillo, M. Tengner, and A. Karlsson, Opt. Express **16**, 9702 (2008).
[23] K. T. Kapale and J. P. Dowling, Phys. Rev. Lett. **99**, 053602 (2007).
[24] K. Thyagarajan, J. Lugani, S. Ghosh, K. Sinha, A. Martin, D. B. Ostrowsky, O. Alibart, and S. Tanzilli, Phys. Rev. A **80**, 052321 (2009).
[25] H. Nishihara, M. Haruna, and T. Suhara, *Optical Integrated Circuits* (McGraw-Hill, New York, 1989).
[26] A. Ghatak, and K. Thyagarajan, *Optical Electronics* (Cambridge University Press, Cambridge, 2007).
[27] [http://www.crystaltechnology.com/docs/LNopt.pdf].
[28] S. Fouchet, A. Carenco, C. Daguet, R. Guglielmi, and L. Riviere, J. Lightwave Technol. **5**, 700 (1987).
[29] M. A. Nielson and I. L. Chuang, *Quantum Computation and Quantum Information* (Cambridge University Press, Cambridge, 2006).
[30] A. Rossi, G. Vallone, A. Chiuri, F. De Martini, and P. Mataloni, Phys. Rev. Lett. **102**, 153902 (2009).